J Mater Sci (2016) 51:10293–10300

Comparative study of fluorite-type ceria-based $Ce_{1-x}Ln_xO_{2-\delta}$ (Ln = Tb, Gd, and Pr) mixed ionic electronic conductors densified at low temperatures

Devaraj Ramasamy[1], Aliaksandr L. Shaula[1], Narendar Nasani[1], Andrei V. Kovalevsky[2], and Duncan P. Fagg[1,*]

[1] *TEMA - Centre for Mechanical Technology and Automation, Department of Mechanical Engineering, University of Aveiro, 3810-193 Aveiro, Portugal*

[2] *CICECO - Aveiro Institute of Materials, Department of Materials and Ceramic Engineering, University of Aveiro, 3810-193 Aveiro, Portugal*

Received: 6 May 2016
Accepted: 23 July 2016
Published online: 1 August 2016

ABSTRACT

It has been reported that peak mixed conducting performance can only be obtained in doped ceria-based fluorite ceramics that contain cobalt sintering additives, when these materials are sintered below 1100 °C. Hence, this article provides a comparative analysis of the electrochemical behavior of such materials formed under the aforementioned conditions. The transport properties of $Ce_{0.8}Tb_{0.2}O_{2-\delta}$ (CTO), $Ce_{0.8}Gd_{0.2}O_{2-\delta}$ (CGO), and $Ce_{0.8}Pr_{0.2}O_{2-\delta}$ (CPO) with 2 mol% Co sintering aid were analyzed for samples prepared and sintered under similar conditions. The total conductivities of these samples were characterized by impedance spectroscopy under air atmosphere in the temperature range of 200–850 °C. Oxide-ion transference numbers were determined by the modified electromotive force method under oxygen/air gradient. Ionic and electronic conductivities were calculated from transference numbers and total conductivity measurements and compared. CTO + Co and CPO + Co ceramic materials show higher relative contribution of the electronic transport compared to CGO + Co. Among these materials, CPO + Co shows the highest total and partial electronic conductivities, as well as the highest oxygen permeability, with essentially the same partial oxide-ion conduction as CGO + Co.

Introduction

Significant scientific effort has been devoted to the study of ceria-based oxides, as they can exhibit ionic conducting, electronically conducting, or mixed conducting properties depending on substitution mechanism, rendering them appropriate for a variety of applications, such as electrolytes and electrodes for solid oxide fuel cells (SOFCs) [1, 2], oxygen sensors [3], oxygen permeation membranes [4], and ultraviolet ray

Address correspondence to E-mail: duncan@ua.pt

DOI 10.1007/s10853-016-0256-2

absorbents [5]. Although perovskite and perovskite-related structure materials have traditionally been the most widely studied as potential mixed conductors [6, 7], significant levels of ambipolar conductivity can also be obtained in materials of the defect cubic fluorite-type structure by substitution of mixed-valence elements in recognized fast ionic conductors, for example, Nb or Ti substitution into zirconia-based fluorites [8, 9], or Pr and Tb into ceria-based fluorites [4, 10, 11]. In the case of the ceria-based materials, such substitution can lead to p-type electronic conductivity in oxidizing conditions via small polaron hopping arising from Pr^{3+}/Pr^{4+} or Tb^{3+}/Tb^{4+} [4, 10, 11], whereas in reducing environment, *n*-type electronic conductivity can also be induced due to partial reduction of Ce^{4+} to Ce^{3+} [12–14]. Additional gains in ambipolar conductivity can also be obtained in oxidizing conditions by the presence of small quantities of sintering additives, where preferential segregation of the additive to grain boundaries has been demonstrated to lead to beneficial effects on the level of electronic conductivity [11, 15–17]. Several transition elements have been reported to show this effect e.g., Cu, Co, and Fe, with the most studied being that of minor cobalt oxide additions (2 mol%), where significantly enhanced densification and improved ambipolar conductivities have been documented for a wide range of $Ce_{1-x}Ln_xO_{2-\delta}$ systems (Ln = Tb, Pr, Gd, La, Eu, Er, Yb, and Nd) [10, 11, 15, 16, 18–21]. Further increases in the amount of sintering additive beyond this level have been reported to be detrimental for conductivity [11, 22]. The concept behind the present study follows from the observation that the sintering temperature of ceria-based materials with Co sintering additives is a critical factor to obtain the desired enhanced electrical performance. Excessive sintering temperatures are shown to lead to grain growth and significant segregation of cobalt into isolated grains, resulting in decreased ambipolar conductivities and oxygen permeation fluxes [17, 20, 23]. Therefore, in the current work, we analyze $Ce_{0.8}Tb_{0.2}O_{2-\delta}$ with small additions (2 mol%) of cobalt oxide sintering aid, sintering at low temperature (<1000 °C) where optimal transport properties are maintained [15, 17, 23]. Electrical conductivity, EMF, and oxygen permeability measurements were performed in order to understand the behavior of CTO mixed ionic electronic conductor. Results were compared to the transference numbers, total and partial ionic and electronic conductivities, and oxygen permeability of cobalt containing $Ce_{0.8}Gd_{0.2}O_{2-\delta}$ and $Ce_{0.8}Pr_{0.2}O_{2-\delta}$ that were prepared under similar low-temperature conditions. In this way, the current article provides a direct appraisal of the peak electrical properties and oxygen permeabilities obtainable from $Ce_{1-x}Ln_xO_{2-\delta}$ (Ln = Tb, Pr, and Gd) materials containing cobalt oxide sintering additives.

Experimental

Cerium terbium oxide ($Ce_{0.8}Tb_{0.2}O_{2-\delta}$) powder was synthesized via the hydrothermal method, with cerium (III) nitrate hexahydrate and terbium (III) nitrate pentahydrate as precursors. The detailed $Ce_{0.8}Tb_{0.2}O_{2-\delta}$ preparation was reported elsewhere [17]. Cerium praseodymium oxide ($Ce_{0.8}Pr_{0.2}O_{2-\delta}$) was produced by the solid-state route from cerium (III) nitrate hexahydrate and praseodymium (III, IV) oxide, as described elsewhere [11]. Commercial cerium gadolinium oxide ($Ce_{0.8}Gd_{0.2}O_{2-\delta}$) was supplied by Rhodia [15]. The cobalt oxide (2 mol%) sintering aid was added in the form of an aqueous solution of cobalt (II) nitrate, followed by ultrasonic treatment, drying and grinding with an agate mortar and pestle. Subsequently, all the powders were dry compacted into pellets at 30–60 MPa and further compressed by isostatic pressing at 200 MPa. The pellets were sintered at 900–1000 °C for 5 h in air.

Powder XRD patterns were acquired in a Rigaku Geigaku Geigerflex diffractometer (Cu Kα radiation) over a 2θ range of 20°–80°. The impedance spectra for pellets with platinum electrodes were recorded by means of Electrochemie-Autolab PGSTAT302 *N* frequency response analyser in the frequency range of 0.01 Hz–1 MHz. The activation energy (E_a) values for the conductivities were calculated by the standard Arrhenius equation,

$$\sigma = \frac{A_0}{T} e^{-\frac{E_a}{RT}}, \quad (1)$$

where A_0 is the pre-exponential factor.

Oxygen ionic transference numbers (t_o) were measured using the modified electromotive force (EMF) method first proposed by Gorelov [24],

$$\frac{E_{obs}}{E_{th}} = t_o \left[1 + \frac{R_\eta}{R_o + R_e}\right]^{-1}, \quad (2)$$

where R_η is the polarization resistance, R_o and R_e are the partial oxygen ionic and electronic resistances of

the sample, respectively [25]. Oxygen permeation measurements for cobalt containing $Ce_{0.8}Pr_{0.2}O_{2-\delta}$ and $Ce_{0.8}Tb_{0.2}O_{2-\delta}$ were performed on dense gas-tight samples following the procedure reported elsewhere [26]. The discussion of the permeation phenomena is based on the oxygen flux density, j, and the specific oxygen permeability, $J(O_2)$, which are interrelated as

$$J(O_2) = jd\left[\ln\frac{p_2}{p_1}\right]^{-1}, \quad (3)$$

where p_1 is the oxygen partial pressure at the membrane permeate (inner) side and p_2 is the oxygen partial pressure at the membrane feed (outer) side remaining constant at $\sim$0.21 atm ($p_1 < p_2$).

The oxygen flux density and specific oxygen permeability values of cobalt containing $Ce_{0.8}Gd_{0.2}O_{2-\delta}$ were calculated using the oxygen ionic transference numbers for oxygen/air gradient, the total conductivity, the relation between $J(O_2)$ and j (Eq. 3), and following relationship between the specific oxygen permeability $J(O_2)$ and the ambipolar conductivity (σ_{amb}) averaged for a given oxygen partial pressure range ($\overline{\sigma_{amb}}$) [11], assuming that the surface oxygen exchange does not limit the oxygen transport through the membrane:

$$J(O_2) = \frac{RT}{16F^2}\overline{\sigma_{amb}} = \frac{RT}{16F^2}\frac{\sigma_o\sigma_e}{\sigma_o+\sigma_e} = \frac{RT}{16F^2}\overline{\sigma_T t_o(1-t_o)}, \quad (4)$$

where t_o is the oxygen ion transference number and σ_T, σ_o and σ_e represent the total, oxygen ionic and electronic conductivities, respectively.

Results and discussion

Structural and microstructural studies

Figure 1 shows the XRD patterns of $Ce_{0.8}Ln_{0.2}O_{2-\delta}$ ceramic samples (Ln = Gd, Pr, and Tb) sintered at low temperatures $\leq$1000 °C with cobalt oxide (2 mol%) sintering aid. The patterns show broad peaks, reflecting that the formed ceramics are constituted by relatively small grains. SEM micrographs of the sintered samples are presented in Fig. 2, and show a very similar microstructure for all samples with submicron grain sizes <200 nm.

The corresponding lattice parameters (refined from the XRD patterns) are summarized in Table 1. All samples showed densities higher than 90 % of the theoretical densities, confirming that dense materials are obtained after sintering at relatively low temperatures (900–1000 °C) by addition of 2 mol% of cobalt oxide as a sintering aid. Although the ionic radii of the lanthanide dopants increase in the sequence Tb < Gd < Pr, for the same 3+ oxidation state, a direct correlation cannot be made with the measured lattice parameters, due to the variable oxidation state of the Tb and Pr cations [27, 28].

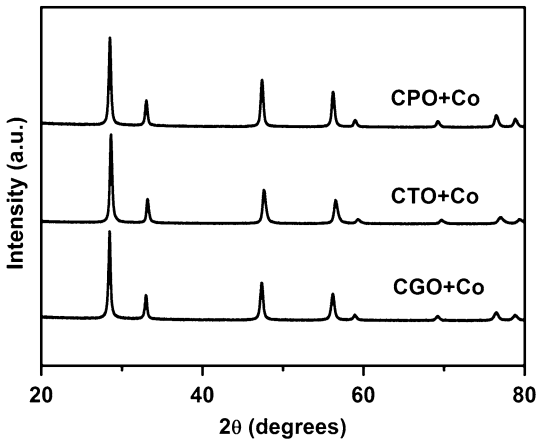

Figure 1 X-ray diffraction patterns of cobalt containing $Ce_{0.8}Ln_{0.2}O_{2-\delta}$ (Ln = Gd, Tb, and Pr) sintered ceramics.

Total conductivity

Figure 3 shows the total conductivities of $Ce_{0.8}Pr_{0.2}O_{2-\delta}$, $Ce_{0.8}Gd_{0.2}O_{2-\delta}$, and $Ce_{0.8}Tb_{0.2}O_{2-\delta}$ ceramics sintered with Co addition, measured in air using impedance spectroscopy. Above 450 °C, the highest total conductivity can be observed for CPO + Co ceramics. Among other two compositions, CGO + Co shows higher total conductivity than CTO + Co in the higher temperature range, while at lower temperatures this tendency is reversed. The activation energies of the total conductivity of these materials, Table 2, show distinct variations between low and high temperature ranges and this feature is more pronounced for materials containing variable valent dopants, Pr and Tb. For these materials, this effect can be related, predominantly, to the changing oxidation states of Pr and Tb with temperature [29].

Partial electronic and oxygen ionic conductivities

Figure 4 represents the behavior of oxygen ionic transference numbers of $Ce_{0.8}Ln_{0.2}O_{2-\delta}$ (Ln = Pr, Tb,

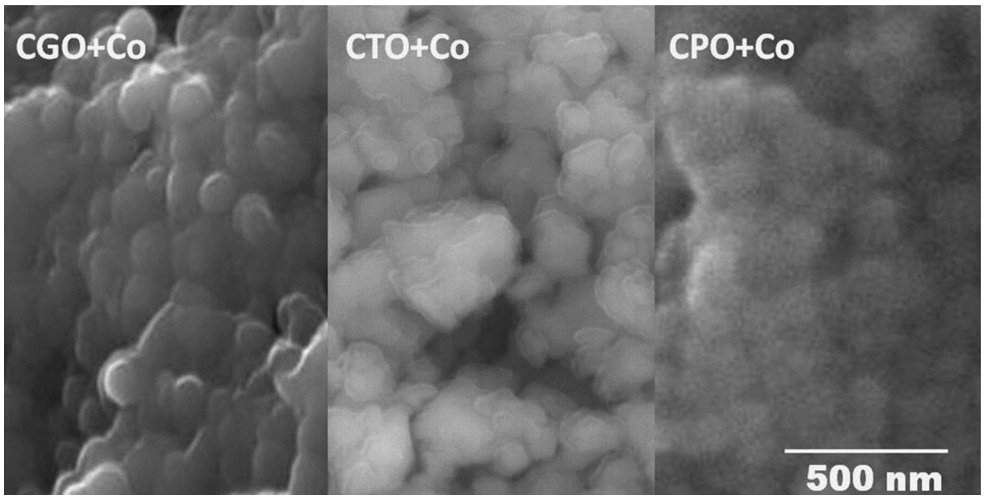

Figure 2 SEM micrographs of sintered ceramics $Ce_{0.8}Ln_{0.2}O_{2-\delta}$ (Ln = Gd, Tb, and Pr) containing cobalt.

Table 1 Lattice parameters of cobalt containing $Ce_{0.8}Ln_{0.2}O_{2-\delta}$ (Ln = Gd, Tb, and Pr) sintered ceramics [11, 15, 17]

Composition	Lattice parameter (Å) (±0.0003)
CGO + Co	5.4275
CTO + Co	5.3910
CPO + Co	5.4106

and Gd) ceramics with Co sintering aid measured by the modified EMF method. The ionic transference numbers were measured across the membrane under $p(O_2)$ gradient (oxygen/air) in the temperature range from 900 to 600 °C. Obtained transference numbers show that CGO + Co and CTO + Co ceramics are predominantly oxygen ionic conductors at these temperatures, in contrast with mixed conducting CPO + Co material. The CGO + Co composition sintered at 900 °C displays oxygen ionic transference numbers that increase with decreasing temperature, approaching unity at the lowest temperature measured. In contrast, the ionic transference numbers of the CPO + Co and CTO + Co compositions are shown to decrease with decreasing temperature.

The combination of ionic transference numbers (t_o) with total conductivity (σ_T), measured in air by impedance spectroscopy at corresponding temperatures, allows the estimation of ionic conductivity (σ_o) through the following relation,

$$\sigma_o = t_o \sigma_T. \quad (5)$$

Figure 5 summarizes the temperature dependencies of the partial oxygen ionic conductivities of these

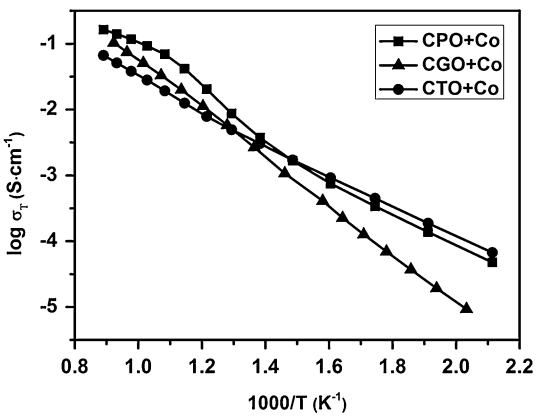

Figure 3 Total conductivity (σ_T) of $Ce_{0.8}Ln_{0.2}O_{2-\delta}$ (Ln = Pr, Tb, and Gd) ceramics with Co sintering aid in air.

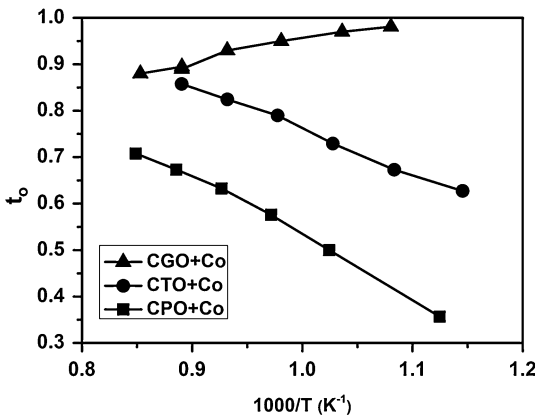

Figure 4 Oxygen ionic transference numbers of $Ce_{0.8}Ln_{0.2}O_{2-\delta}$ (Ln = Pr, Tb, and Gd) ceramics with Co sintering aid, measured in oxygen/air gradient.

Table 2 Activation energy values for the total conductivity of $Ce_{0.8}Ln_{0.2}O_{2-\delta}$ (Ln = Pr, Tb, and Gd) ceramics with Co measured in air

Composition	Activation energy (eV)	
	500–850 °C	200–500 °C
CGO + Co	0.77 ± 0.02	0.79 ± 0.02
CTO + Co	0.64 ± 0.01	0.50 ± 0.01
CPO + Co	0.70 ± 0.12	0.59 ± 0.06

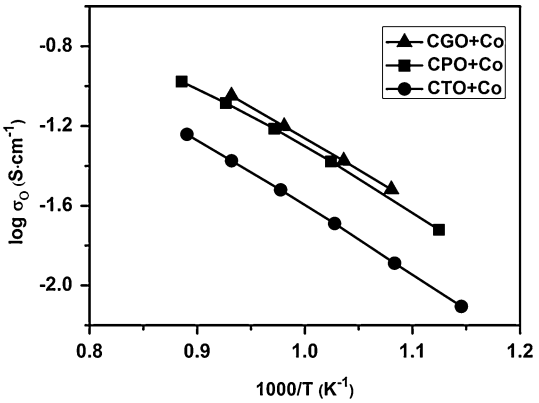

Figure 5 Oxygen ionic conductivities of $Ce_{0.8}Ln_{0.2}O_{2-\delta}$ (Ln = Pr, Tb, and Gd) ceramics with Co sintering aid in air.

materials, resulting from Eq. (5). The compositions CGO + Co and CPO + Co show similar levels of ionic conductivity that are considerably higher than that offered by the terbium doped, CTO + Co, composition. All compositions show similar activation energies for ionic conductivity in the studied temperature range, Table 3.

In a similar way, the electronic conductivity can be estimated from oxygen ionic transference numbers and total conductivity values at corresponding temperatures as follows:

$$\sigma_e = (1 - t_o)\sigma_T. \quad (6)$$

Table 3 Activation energy values for the ionic and electronic conductivities in air and oxygen permeation (at $\log(p_2/p_1) \approx 0.7$) of $Ce_{0.8}Ln_{0.2}O_{2-\delta}$ (Ln = Pr, Tb, and Gd) ceramics with Co

Composition	Activation energy (eV)		
	Ionic	Electronic	Oxygen permeation
CGO + Co	0.71 ± 0.01	1.50 ± 0.20	1.56 ± 0.20
CTO + Co	0.75 ± 0.02	0.32 ± 0.08	0.43 ± 0.04
CPO + Co	0.69 ± 0.04	0.23 ± 0.01	0.49 ± 0.09

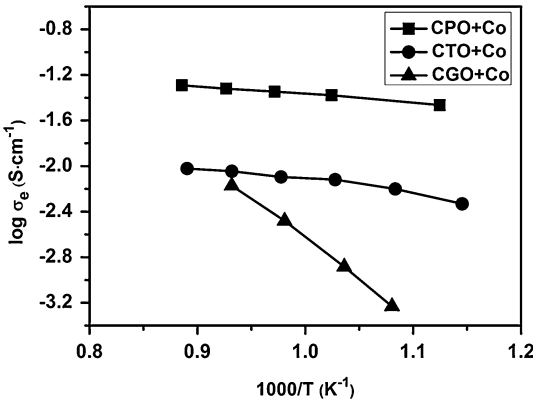

Figure 6 Electronic conductivities of $Ce_{0.8}Ln_{0.2}O_{2-\delta}$ (Ln = Pr, Tb, and Gd) ceramics with Co sintering aid in air.

It has been reported that the addition of 2 mol% CoO into $Ce_{0.8}Gd_{0.2}O_{2-\delta}$, $Ce_{0.8}Tb_{0.2}O_{2-\delta}$, and $Ce_{0.8}Pr_{0.2}O_{2-\delta}$ systems can lead to enhancement of p-type electronic conductivities over the base compositions and this enhancement is greatest for materials sintered at low temperatures (900–1000 °C) [17, 20, 23]. For these peak performing materials, Fig. 6 shows that the highest electronic conductivities are offered by the compositions containing the variable valent lanthanide dopants, Pr and Tb. The highest electronic contribution of all materials studied is offered by the composition CPO + Co. The activation energies of the electronic conductivity of the CPO + Co and CTO + Co compositions are shown to be similar and to be lower than that of the CGO + Co material (Table 3).

Oxygen permeation fluxes

Figure 7a, b shows, respectively, the oxygen flux density, j, and specific oxygen permeability, $J(O_2)$, for the CTO + Co, CPO + Co, and CGO + Co compositions at various temperatures, as a function of the oxygen partial pressure gradient. Previous literature has shown that oxygen surface exchange limitations are insignificant for 2 mol% cobalt oxide containing CTO [17, 19] and CPO [11] materials, in the studied temperature range. Moreover, considering that increased mixed conductivity and faster oxygen surface exchange have been reported that for ceria-based oxides when the grain size decreases to the submicron range [26, 30], the surface kinetics of 2 mol% cobalt oxide containing CGO is assumed to not significantly limit the oxygen permeation for the

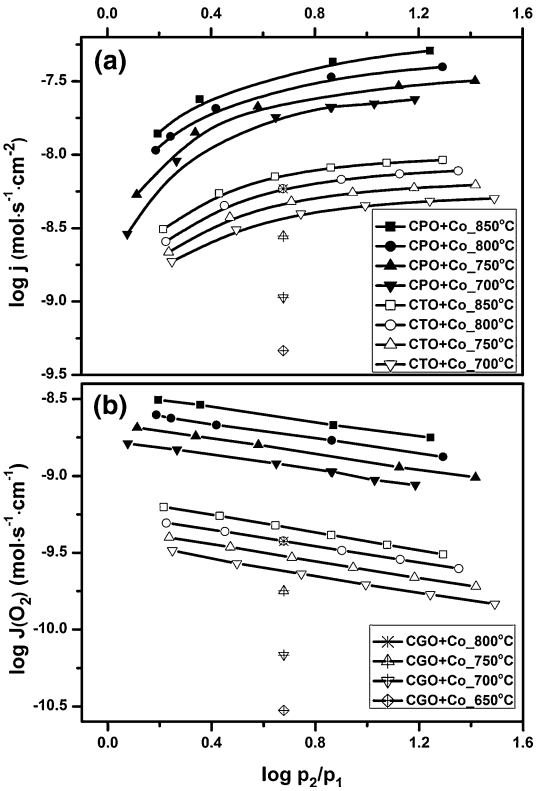

Figure 7 The steady-state oxygen permeation fluxes (**a**) and specific oxygen permeability values (**b**) for cobalt containing $Ce_{0.8}Ln_{0.2}O_{2-\delta}$ (Ln = Pr, Tb, and Gd) 1 mm thick membranes versus oxygen partial pressure gradient (for Pr and Tb-measured, for Gd-calculated).

following comparison; the results presented for this composition in Fig. 7 should, therefore, be considered as a best case scenario. The oxygen permeation flux and, consequently, specific permeability values of cobalt containing $Ce_{0.8}Pr_{0.2}O_{2-\delta}$ are substantially higher than those of cobalt added $Ce_{0.8}Tb_{0.2}O_{2-\delta}$ and $Ce_{0.8}Gd_{0.2}O_{2-\delta}$ for these peak performing materials sintered at low temperatures. As shown in Eq. (4), higher partial oxygen ionic and electronic conductivities result in higher oxygen permeability (assuming negligible surface exchange limitations), achieving a maximum when these conductivities are similar ($t_o = 0.5$). Indeed, cobalt containing $Ce_{0.8}Pr_{0.2}O_{2-\delta}$ offers a better combination of the oxygen ionic transference number (Fig. 4) and partial conductivities (Figs. 5, 6), when compared with that offered by CTO + Co and CGO + Co.

At 800 °C, the oxygen permeability values of cobalt containing $Ce_{0.8}Tb_{0.2}O_{2-\delta}$ and $Ce_{0.8}Gd_{0.2}O_{2-\delta}$ are very close (Fig. 7), reflecting that their ambipolar conductivities ($\overline{\sigma_{amb}} = \frac{\sigma_o\sigma_e}{\sigma_o+\sigma_e}$) at this temperature are similar. Thus, although the oxygen ionic conductivity of CGO + Co is noted to be significantly higher than that of CTO + Co (Fig. 5), its ambipolar conductivity is limited by a low level of electronic conduction that is inferior to that offered by the CTO + Co composition under these conditions (Fig. 6). On decreasing temperature, the difference in electronic conductivity between these two oxides increases (Fig. 6), as the activation energy of electronic conduction for CGO + Co is considerably higher than that of CTO + Co (Table 3). Thus, at lower temperatures, the lower electronic component in the CGO + Co case can no longer be compensated (in terms of ambipolar conductivity) by ionic conductivity due to the similar activation energies for ionic conductivity of these materials (Table 3). As a consequence, the oxygen permeation of cobalt containing $Ce_{0.8}Gd_{0.2}O_{2-\delta}$ becomes progressively lower than that of cobalt added $Ce_{0.8}Tb_{0.2}O_{2-\delta}$, upon decreasing temperature (Fig. 7).

On consideration of the definition of ambipolar conductivity ($\overline{\sigma_{amb}} = \frac{\sigma_o\sigma_e}{\sigma_o+\sigma_e}$), it becomes clear that if one of the partial conductivities is significantly lower than the other one (e.g., for CGO + Co, $\sigma_e \ll \sigma_o$), the ambipolar conductivity and, therefore, oxygen permeation become limited by this contribution (for example in the case of CGO + Co, limitation in ambipolar conductivity is by the level of electronic transport: $\overline{\sigma_{amb}} \approx \sigma_e$). In agreement, the activation energy of oxygen permeation flux through cobalt containing $Ce_{0.8}Gd_{0.2}O_{2-\delta}$ membrane, determined according to the standard Arrhenius equation [see Eq. (1) as a model], is very similar to the activation energy of its electronic transport (Table 3), further highlighting that the oxygen permeability of CGO + Co is mostly limited by its bulk electronic conduction.

The activation energy values of oxygen permeation flux for cobalt containing $Ce_{0.8}Pr_{0.2}O_{2-\delta}$ and $Ce_{0.8}Tb_{0.2}O_{2-\delta}$ lie between their respective activation energy values for oxygen ionic and electronic conductivities, being slightly closer to the activation energy of electronic transport (Table 3). This indicates that the oxygen permeability of CPO + Co and CTO + Co, contrary to CGO + Co, is governed by both partial conductivities. The oxygen ionic transference numbers (Fig. 4) confirm this assumption, as t_o values of cobalt containing $Ce_{0.8}Pr_{0.2}O_{2-\delta}$ and

$Ce_{0.8}Tb_{0.2}O_{2-\delta}$ are considerably closer to 0.5, than those of cobalt added $Ce_{0.8}Gd_{0.2}O_{2-\delta}$.

Conclusions

The introduction of small amount (2 mol%) of cobalt oxide is highly effective as a sintering aid in fluorite $Ce_{1-x}Ln_xO_{2-\delta}$ (Ln = Tb, Gd, and Pr) oxides allowing dense materials with submicron grain sizes to be formed at sintering temperatures of 1000 °C and below. For the peak performing samples prepared under these conditions, ambipolar conductivities are shown to increase in the order CGO + Co < CTO + Co < CPO + Co. The oxygen ion transference number of CTO + Co, obtained from modified EMF method, increases with temperature, in line with that observed for the praseodymium-substituted composition CPO + Co. In contrast, the oxygen ion transference number of the gadolinium substituted analogue, CGO + Co, exhibits negative temperature dependence. The ambipolar conductivities of CTO + Co and CGO + Co compositions are observed to be similar at the highest temperatures studied, 800 °C, while deviating strongly with decreasing temperature due to a much greater activation energy for the electronic conductivity component in the CGO + Co case. The oxygen permeabilities obtainable from these materials follow these trends, increasing in the sequence CGO + Co < CTO + Co < CPO + Co. The current work shows that the $Ce_{0.8}Tb_{0.2}O_{2-\delta}$ with low concentration of Co sintering additive can attain relatively high mixed ionic electronic conductivity after sintering at low temperature of 900 °C. Nonetheless, this performance is shown to be significantly inferior to that offered by the praseodymium-substituted material, CPO + Co.

Acknowledgements

The authors gratefully acknowledge funding from the FCT, FEDER, COMPETE, POPH, FCT Investigator Programme, Projects POCI-01-0145-FEDER-007679, POCI-01-0145-FEDER-016756 (FCT Refs. UID /CTM /50011/2013, PTDC/CTM-ENE/6319/2014, IF/00280/2012 and PEst-C/EME/UI0481/2013, Portugal and the European Social Fund, European Union.

References

[1] Zhang TS, Ma J, Leng YJ, Chan SH, Hing P, Kilner JA (2004) Effect of transition metal oxides on densification and electrical properties of Si-containing $Ce_{0.8}Gd_{0.2}O_{2-\delta}$ ceramics. Solid State Ionics 168:187–195

[2] Martínez-Arias A, Hungría AB, Fernández-García M, Iglesias-Juez A, Conesa JC, Mather GC, Munuera G (2005) Cerium-terbium mixed oxides as potential materials for anodes in solid oxide fuel cells. J Power Sour 151:43–51

[3] Jasinski P, Suzuki T, Anderson HU (2003) Nanocrystalline undoped ceria oxygen sensor. Sens Actuators B 95:73–77

[4] Chatzichristodoulou C, Hendriksen PV (2012) Electronic and ionic transport in $Ce_{0.8}Pr_xTb_{0.2-x}O_{2-\delta}$ and evaluation of performance as oxygen permeation membranes. ECS Trans 45:45–62

[5] Morimoto T, Tomonaga H, Mitani A (1999) Ultraviolet ray absorbing coatings on glass for automobiles. Thin Solid Films 351:61–65

[6] Shin MJ, Yu JH (2012) Oxygen transport of A-site deficient $Sr_{1-x}Fe_{0.5}Co_{0.5}O_{3-\delta}$ ($x = 0-0.3$) membranes. J Membr Sci 401:40–47

[7] Kim JJ, Kuhn M, Bishop SR, Tuller HL (2013) Cathodic and defect properties of $Ba_xSr_{1-x}Ti_{1-y}Fe_yO_{3-y/2+\delta}$ mixed conducting oxides. Solid State Ionics 230:2–6

[8] Fagg D, Feighery A, Irvine JT (2003) The systems Zr(Nb, Ti)(R)$O_{2-\delta}$, R = Yb, Ca—optimization of mixed conductivity and comparison with results of other systems (R = Y and Gd). J Solid State Chem 172:277–287

[9] Tao S, Irvine JTS (2002) Optimization of mixed conducting properties of Y_2O_3–ZrO_2–TiO_2 and Sc_2O_3–Y_2O_3–ZrO_2–TiO_2 solid solutions as potential SOFC anode materials. J Solid State Chem 165:12–18

[10] Balaguer M, Solís C, Serra JM (2012) Structural–transport properties relationships on $Ce_{1-x}Ln_xO_{2-\delta}$ system (Ln = Gd, La, Tb, Pr, Eu, Er, Yb, Nd) and effect of cobalt addition. J Phys Chem C 116:7975–7982

[11] Fagg DP, García-Martin S, Kharton VV, Frade JR (2009) Transport properties of fluorite-type $Ce_{0.8}Pr_{0.2}O_{2-\delta}$: optimization via the use of cobalt oxide sintering aid. Chem Mater 231:381–391

[12] Blumenthal RN, Panlener RJ (1970) Electron mobility in nonstoichiometric cerium dioxide at high temperatures. J Phys Chem Solids 31:1190–1192

[13] Tuller HL, Nowick AS (1977) Small polaron electron transport in reduced CeO_2 single crystals. J Phys Chem Solids 38:859–867

[14] Naik IK, Tien TY (1978) Small-polaron mobility in nonstoichiometric cerium dioxide. J Phys Chem Solids 39:311–315

[15] Fagg D, Abrantes JC, Pérez-Coll D, Núñez P, Kharton V, Frade J (2003) The effect of cobalt oxide sintering aid on electronic transport in $Ce_{0.80}Gd_{0.20}O_{2-\delta}$ electrolyte. Electrochim Acta 48:1023–1029

[16] Fagg DP, Kharton VV, Frade JR (2003) p-Type electronic transport in $Ce_{0.8}Gd_{0.2}O_{2-\delta}$: the effect of transition metal oxide sintering aids. J Electroceram 9:199–207

[17] Ramasamy D, Shaula AL, Gómez-Herrero A, Kharton VV, Fagg DP (2015) Oxygen permeability of mixed-conducting $Ce_{0.8}Tb_{0.2}O_{2-\delta}$ membranes: effects of ceramic microstructure and sintering temperature. J Membr Sci 475:414–424

[18] Applicata C (1992) Sintering aids for ceria-zirconia alloys. J Mater Sci 27:2734–2738. doi:10.1007/BF00540698

[19] Balaguer M, Solís C, Serra M (2011) Study of the transport properties of the mixed ionic electronic conductor $Ce_{1-x}Tb_xO_{2-\delta}$ + Co ($x = 0.1$, 0.2) and evaluation as oxygen-transport membrane. Chem Mater 23:2333–2343

[20] Pérez-Coll D, Núñez P, Abrantes J, Fagg D, Kharton V, Frade J (2005) Effects of firing conditions and addition of Co on bulk and grain boundary properties of CGO. Solid State Ionics 176:2799–2805

[21] Fagg DP, Kharton VV, Frade JR (2004) Transport in ceria electrolytes modified with sintering aids: effects on oxygen reduction kinetics. J Solid State Electrochem 8:618–625

[22] Baral AK, Dasari HB, Kim B, Lee J (2013) Effect of sintering aid (CoO) on transport properties of nanocrystalline Gd doped ceria (GDC) materials prepared by co-precipitation method. J Alloys Compd 575:455–460

[23] Balaguer M, Solís C, Roitsch S, Serra JM (2014) Engineering microstructure and redox properties in the mixed conductor $Ce_{0.9}Pr_{0.1}O_{2-\delta}$ + Co 2 mol%. Dalton Trans 4:4305–4312

[24] Gorelov VP (1988) Transference number determination in ionic conductors by the e.m.f. method with active load. Elektrokhimiya 24:1380–1381

[25] Kharton VV, Marques FMB (2001) Interfacial effects in electrochemical cells for oxygen ionic conduction measurements. I. The e.m.f. method. Solid State Ionics 140:381–394

[26] Tikhonovich VV, Shuangbao L, Naumovich EN, Kovaievsky AV, Viskup AP, Bashmakov IA, Yaremchenko AA (1998) Ceramic microstructure and oxygen permeability of SrCo(Fe, M)$O_{3-\delta}$ (M = Cu or Cr) perovskite membranes. J Electrochem Soc 145:1363–1373

[27] Coduri M, Scavini M, Brunelli M, Pedrazzin E, Masala P (2014) Structural characterization of Tb- and Pr-doped ceria. Solid State Ionics 268:150–155

[28] Fagg D, Kharton V, Shaula A, Marozau I, Frade J (2005) Mixed conductivity, thermal expansion, and oxygen permeability of Ce(Pr, Zr)$O_{2-\delta}$. Solid State Ionics 176:1723–1730

[29] Fagg DP, Marozau IP, Shaula AL, Kharton VV, Frade JR (2006) Oxygen permeability, thermal expansion and mixed conductivity of $Gd_xCe_{0.8-x}Pr_{0.2}O_{2-\delta}$, $x = 0$, 0.15, 0.2. J Solid State Chem 179:3347–3356

[30] Kosacki I, Anderson HU (2000) Microstructure–property relationships in nanocrystalline oxide thin films. Ionics 6:294–311